Nanoscale Res Lett (2010) 5:1301–1306
DOI 10.1007/s11671-010-9642-x

NANO EXPRESS

Synthesis and Characterization of Cobalt-Doped WS_2 Nanorods for Lithium Battery Applications

Shiquan Wang · Guohua Li · Guodong Du · Li Li · Xueya Jiang · Chuanqi Feng · Zaiping Guo · Seungjoo Kim

Received: 16 March 2010 / Accepted: 7 May 2010 / Published online: 23 May 2010

Abstract Cobalt-doped tungsten disulfide nanorods were synthesized by an approach involving exfoliation, intercalation, and the hydrothermal process, using commercial WS_2 powder as the precursor and *n*-butyllithium as the exfoliating reagent. XRD results indicate that the crystal phase of the sample is 2H-WS_2. TEM images show that the sample consists of bamboo-like nanorods with a diameter of around 20 nm and a length of about 200 nm. The Co-doped WS_2 nanorods exhibit the reversible capacity of 568 mAh g^{-1} in a voltage range of 0.01–3.0 V versus Li/Li^+. As an electrode material for the lithium battery, the Co-doped WS_2 nanorods show enhanced charge capacity and cycling stability compared with the raw WS_2 powder.

Keywords Tungsten disulfide · Chemical synthesis · Electrochemical properties · Electrode materials · Hydrothermal method

S. Wang · L. Li · X. Jiang · C. Feng
Department of Chemistry, Hubei University, Wuhan 430062, People's Republic of China

G. Li
State Key Laboratory Breeding Base of Green Chemistry-Synthesis Technology, Zhejiang University of Technology, Hangzhou 310032, People's Republic of China

G. Du · Z. Guo (✉)
School of Mechanical, Materials & Mechatronics, Institute for Superconducting & Electronic Materials, Faculty of Engineering, University of Wollongong, Wollongong, NSW 2522, Australia
e-mail: zguo@uow.edu.au

S. Wang · S. Kim
Institute of NT-IT Fusion Technology, Division of Energy Systems Research, Ajou University, Suwon 443-749, Republic of Korea

Introduction

Due to its distinctive layer structure and electronic properties, the inorganic fullerene-like structure of MS_2(M = Mo, W) has been attracting considerable attention and has been investigated extensively for various applications. The properties of the metal disulfide nanomaterials with novel morphology are better than those of their bulk forms. WS_2 and MoS_2 nanomaterials have shown excellent properties and have potential applications in various fields, such as scanning probe microscopy [1], solid-state lubricants [2], heterogeneous catalysis [3], and electrochemical hydrogen storage [4]. In order to investigate their properties and applications in these fields systematically, several methods have been reported to prepare nanoscale MS_2, such as gas–solid or gas phase reaction [5], pulsed laser deposition [6], a self-transformation process [7], and sulfidation of the MoO_3 nanofibers under a H_2S/H_2 steam at 350–600°C [8]. However, almost all the methods are based on utilizing high temperature reactions or dangerous gases, such as H_2 and H_2S. On the other hand, the formation of nanosized MoS_2 or WS_2 polyhedral or onion crystals is, similar to the case of carbon onion crystals, a rare event [9]. From this point of view, it is interesting and valuable to find a new large-scale approach to synthesize metal disulfide nanoparticles.

Since the 1970s, lamellar disulfide has been intensively studied, especially via the intercalation technique [10–12]. During intercalation, the coordination patterns of lamellar disulfide change greatly, and numerous defects are introduced, which enable doping of other ions [13, 14]. On the other hand, after transition metal cations have entered the WS_2 or MoS_2 matrix, there are changes in the bonding properties of the matrix and the S–M–S bond angles [14–16]. Golub et al. [16] described room temperature preparation of new ternary metal sulfides M_xMoS_2

(M = Cu, Ag) by exfoliation–restacking technique. First, the MoS_2 powder is exfoliated into lamellae or monolayers by *n*-butyllithium to form Li_xMoS_2. Then $(MoS_2)^{x-}$ is formed by the reaction of Li_xWS_2 with water. They supposed that ternary metal sulfides M_xMoS_2 could be obtained using $(MoS_2)^{x-}$ single layers dispersed in aqueous media and salts of metals which could favor the formation of M–S rather than M–O(OH, H_2O) bonds. Thus, the $(MoS_2)^{x-}$ single layers in the dispersions have henceforth to be considered not only as macroanions but also as reducing agents. For the MoS_2, the negative charge of $(MoS_2)^{x-}$ and consequently the cluster structure of S–Mo–S layers with Mo–Mo metal bonding can be effectively stabilized in restacked compounds by introduction into the structure of counterions covalently bonded to the matrix. So it is possible the same reason for the WS_2, the introduction of cobalt ion into the matrix of WS_2 can stabilize the WS_2. Li et al. [17, 18] utilized these bond changes and fabricated transition metal-doped disulfide nanotubes successfully by exfoliation–intercalation through hydrothermal adulteration, using lamellar metal disulfide as the precursors.

WS_2 and MoS_2 could be electrode materials for rechargeable batteries due to the existence of van der Waals forces across the gaps between the S–M–S sheets, which can provide the space for guest reactants in intercalation reactions [19]. A few attempts have been made to investigate the electrochemical activity of MS_2 (M = Mo, W, etc.) electrodes. For example, Feng [20] reported that WS_2 nanoflakes prepared by a rheological phase reaction had better lithium intercalation/deintercalation behavior than other forms of WS_2. Wang [21] prepared WS_2 nanotubes and reported that the WS_2 nanotube electrode delivered a lithium insertion capacity of 915 mAh g^{-1}, which is much higher than for WS_2 powder.

As other approach to explore new electrode materials for Li-battery, nanosized transition metal oxides have been attracting much attention in recent years. Poizot et al. [22] reported the high performance as anode materials in lithium ion batteries for nanosized transition metal oxides such as nickel oxide, cobalt oxide, and iron oxide. Among them, cobalt oxide demonstrated the best electrochemical properties. In this regard, Co-containing species can be promising intercalants to modify the lamellar disulfides. In this paper, bamboo-like Co-doped WS_2 nanorods were synthesized on a large scale by an approach involving exfoliation–intercalation–hydrothermal treatment, using lamellar tungsten disulfide as the precursor, and the morphology, chemical components, and Raman spectrum are reported. The cobalt-doped WS_2 nanorods can reversibly store lithium with a capacity of 568 mAh g^{-1} over a voltage range of 0.01–3.0 V versus Li/Li^+ and show good cycling stability. To the best of our knowledge, this is the first time that transition metal-doped WS_2 nanorods have been synthesized and their applications in lithium ion batteries systematically investigated.

Experimental

Sample Preparation

Under N_2 atmosphere at room temperature for a week, 8.2 g of WS_2 powder was exfoliated by 2.9 M of *n*-butyllithium (15 ml) in a container, rinsed in hexane six times, and vacuum dried at 80°C overnight. Then, 0.6 g of Li_xWS_2 was put into a 50 ml autoclave with a Teflon-lined inner wall, and 30 ml of 0.2 M $CoCl_2$ aqueous solution was added into the autoclave and stirred for 15 min. The temperature of the autoclave was raised to 180°C, and it was maintained at that temperature for 48 h before being cooled down to room temperature. The products were filtrated, rinsed in deionized water several times, and dried at 80°C overnight.

Characterization

X-ray diffraction (XRD) was performed with a Rigaku X-ray diffractometer at room temperature, using a quartz monochromator Cu Kα radiation source ($\lambda = 0.1541$ nm) under a voltage of 40 kV and a current of 30 mA. Transmission electron microscopy (TEM) was performed with a FEI/TECNAI G^2 microscope. Before characterization, the samples were dispersed ultrasonically in ethanol and dropped onto a Cu grid coated with a carbon membrane. Energy-dispersive X-ray spectroscopy (EDX) was performed on an S-4800 scanning electron microscope. Raman spectra were collected under ambient conditions using a RM 2000 microscope confocal Raman spectrometer equipped with a microscope (Renishaw PLC, England). Electrochemical measurements were carried out using a 2032-type coin cell fabricated in an argon-filled glove box (Mbraun, Germany). The working electrode was fabricated in the ratio of 70:20:10 (w/w) active material/carbon black/polyvinylidene difluoride, while lithium foil served as counter and reference electrode. The electrolyte was 1 M $LiPF_6$ dissolved in 1:1 ethylene carbonate (EC) and dimethyl carbonate (DMC). Constant current charge/discharge cycling was conducted on a LAND battery tester (CT2001A) in the voltage range between 3.0 and 0.01 V. Cyclic voltammetry (CV) was performed on a CHI660C electrochemical workstation at a scan rate of 0.1 mV s^{-1}.

Results and Discussions

Figure 1 shows the XRD patterns of the raw WS_2 powder and the Co-doped WS_2 nanorods. All the peaks are

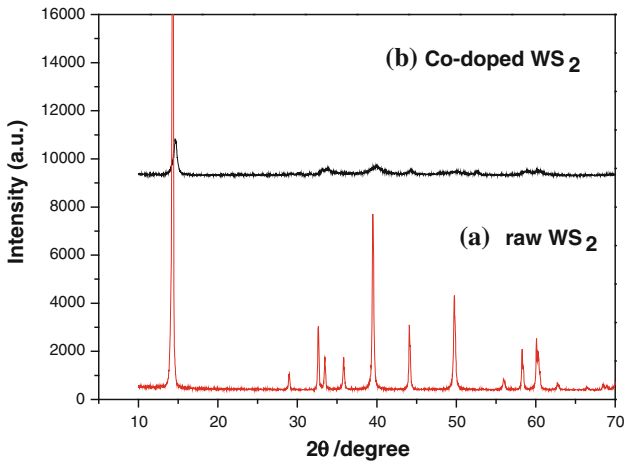

Fig. 1 XRD patterns of the raw WS_2 powder (**a**) and the Co-doped WS_2 sample (**b**)

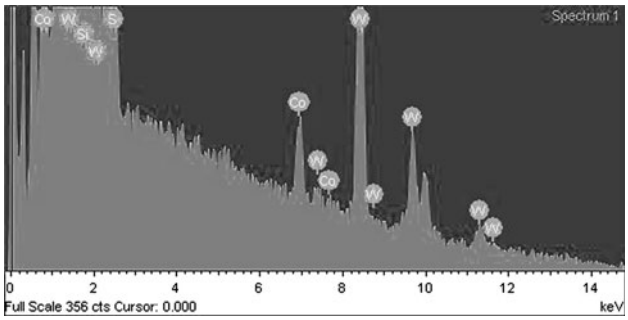

Fig. 2 EDX results on Co-doped WS_2 nanorods. The silicon peak comes from silicon wafer supporting the sample

agreement with the Bragg positions for a hexagonal structure (JCPDS card 08-0237) for both samples. The Co-doped WS_2 nanorods, however, show significantly broadened peak shapes, indicating that the crystallite size is much smaller than that of the raw WS_2 powder. The EDX analysis (Fig. 2) indicates that these nanorods have a Co:W:S atomic ratio of 3.54:31.4:58.03. Taking into account the error of the measurement, the chemical formula of the nanorods is close to $Co_{0.11}WS_2$.

Figure 3a shows a TEM image of the raw WS_2 particles. The morphology is plate-like with a typical diameter around 2.0 μm. The selected area electron diffraction (SAED) pattern reveals that the raw WS_2 consists of single crystals of 2H-WS_2. As shown in Fig. 3b, the morphology of the Co-doped WS_2 particles is that of bamboo-like nanorods with a diameter of about 20 nm and a length of around 200 nm, so the aspect ratio of these nanorods is about 10. The corresponding SAED pattern reveals that the nanorods are polycrystalline 2H-WS_2, which is different from the raw WS_2 particles. The nanorods have somewhat irregular shape, in which the ends of a nanorod are smaller in diameter than its middle part, as shown in Fig. 3c, d.

The Raman spectrum of the sample was collected using a He/Ne laser with a wavelength of 632.8 nm, which is capable of supplying power of 1 mW. The Raman spectrum of the Co-doped WS_2 nanorods displays two peaks around 348.6 and 419.6 cm^{-1}, and no other additional peaks are observed, as shown in Fig. 4. This result is similar to that for WS_2 bulk material and is consistent with reference [23], indicating the local lattice structure of the Co-doped nanorods is comparable with that of the bulk WS_2 crystals in spite of its poor crystallinity.

The electrochemical properties of the Co-doped WS_2 nanorods were compared with those of the raw WS_2 powder. Figure 5a, b show cyclic voltammograms for the two samples. In the first cycle, a reduction peak is observed at ~0.55 V and an oxidation peak at ~2.4 V for both samples. The reduction and the oxidation peaks correspond to Li^+ lithium intercalation/deintercalation behavior in WS_2 for two samples, respectively, as described in Eq. (1).

$$x\,\mathrm{Li} + \mathrm{WS_2} \leftrightarrow \mathrm{Li}_x\mathrm{WS_2} \tag{1}$$

In the second cycle, the reduction peak at 0.55 V has disappeared, while new reduction peaks appear in the potential range from 1.6–2.2 V. This change can be explained by the formation of a gel-like polymeric layer [24]. There was no significant change in the potentials of the redox peaks afterward for Co-doped WS_2. The main difference between two cyclic voltammograms is the relative change in the redox current with the cycle number; the current of the redox peak for the Co-doped WS_2 electrode decreases more slowly than that of the raw WS_2 electrode. As a result, a better cycling performance can be obtained from the Co-doped WS_2 electrode, as shown in Fig. 6a.

Figure 5c shows cyclic voltammograms of the Co-doped WS_2 at potential scan rates, υ, from 20 to 500 μV s^{-1}. The relationship between the oxidation current peak values and $\upsilon^{1/2}$ is depicted in Fig. 5d. The peak currents are proportional to $\upsilon^{1/2}$, which may indicate a semi-infinite diffusion mechanism on the electrode [25]. The relationship to peak current I_p can be expressed by the classical Sevcik equation:

$$I_p = 2.69 \times 10^5 n^{3/2} A D_0^{1/2} \upsilon^{1/2} \Delta c_0 \tag{2}$$

where n is the number of electrons per species reaction, A is the apparent surface area of the electrode, D_0 is the diffusion coefficient of Li^+ in the solid state, υ is the scan rate, and Δc_0 is the change in Li concentration in the active material.

Figure 6a shows the charge/discharge curves of the electrode containing the Co-doped WS_2 nanorods. In the first cycle, the WS_2 electrode delivered a lithium insertion capacity of about 668 mAh g^{-1} when the discharge/charge current density was 50 mA g^{-1}. The first discharge curve

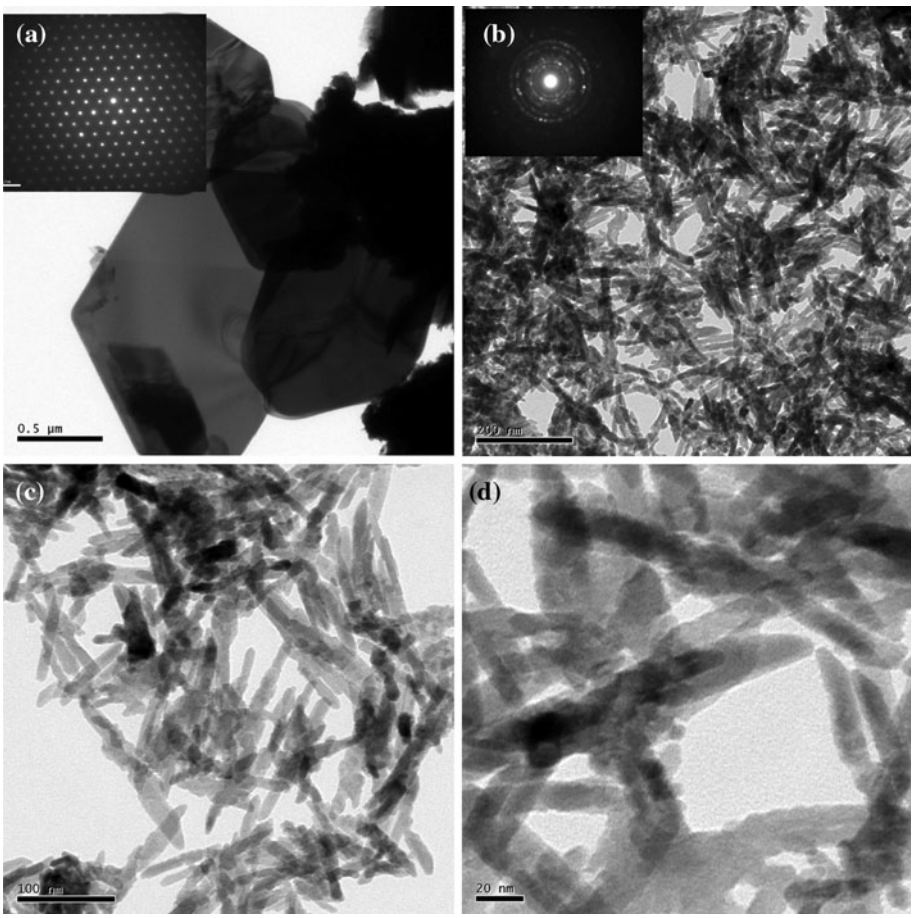

Fig. 3 TEM images of the raw WS_2 (**a**), the Co-doped WS_2 (**b**), and the Co-doped WS_2 at higher magnification (**c**, **d**). The *insets* in **a** and **b** show the corresponding SAED patterns

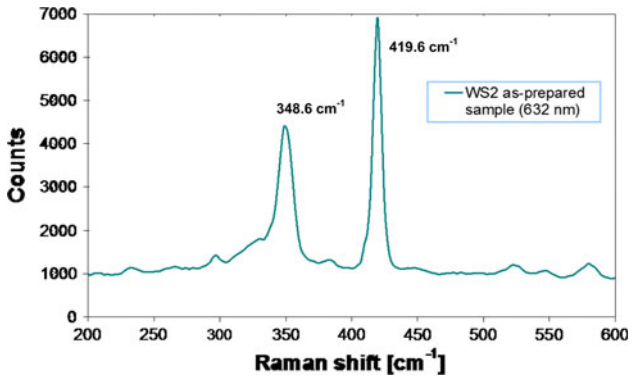

Fig. 4 Raman spectrum of Co-doped WS_2 nanorods

shows the insertion plateaus at 1.0 V and 0.75 V. In the second cycle, a lithium insertion plateau at ~2.2 V was observed, as well as a slope starting from 1.75 V and running down to the cut off voltage of 0.01 V. There is a clear distinction in the charge–discharge profile between 0–2 V (~300 mAh g^{-1}) and 2–3 V (~250 mAh g^{-1}). Thus, this material can be regarded as a possible anode material for Li-ion battery in the 0–2 V range and as a cathode material in Li-metal cell technology.

The cycling behavior over 40 cycles is shown in Fig. 6b. For the raw WS_2, the charge capacity obviously decreases with cycling, from 520 mAh g^{-1} for the first cycle to 287 mAh g^{-1} at the 40th cycle. (The capacity retention is ~55% after 40 cycles.) For the Co-doped WS_2 electrode, an irreversible capacity of 668 mAh g^{-1} is observed in the first cycle, along with a reversible capacity of 568 mAh g^{-1}, which is reduced to 446 mAh g^{-1} after 20 cycles and 380 mAh g^{-1} after 40 cycles. The Co-doped WS_2 electrode shows a better cycling stability compared with the WS_2 precursor electrode. The first cycle coulombic efficiency of the raw WS_2 is 81.5%, and it increases with the cycle number, reaching 98.2% by the 40th cycle. For the Co-doped WS_2, the coulombic efficiency of the first cycle is 84.7% and over 98% from the 4th cycle, shown in Fig. 6c. The improved electrochemical performance of the Co-doped WS_2 sample may be attributed to the small particle size and its one-dimensional structure. However, the charge/discharge capacities of the Co-doped WS_2 electrode are lower than those reported for WS_2 nanoflakes [19] and WS_2 nanotubes [20].

The formation mechanism for the nanorods is similar to the synthesis of transition metal-doped $Mo_xW_{1-x}S_2$ nanotubes [17, 18]. First, the WS_2 powder is exfoliated into

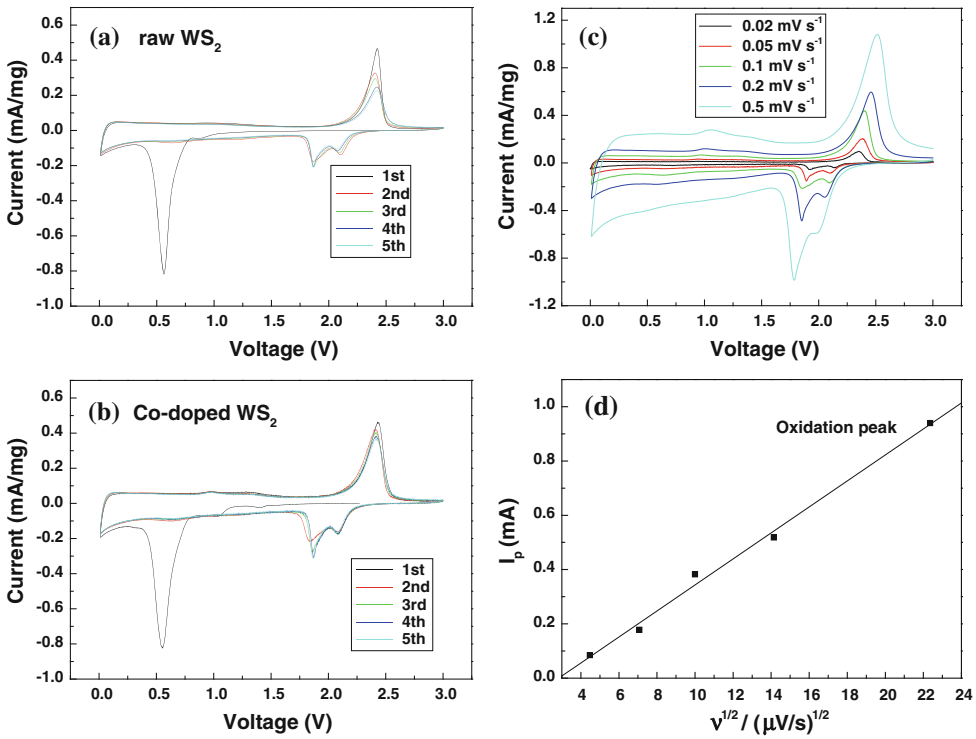

Fig. 5 Cyclic voltammograms of a coin cell (vs. Li) for selected cycles of the raw WS_2 electrode (**a**), the Co-doped WS_2 electrode (**b**), and the Co-doped WS_2 at different potential scan rates υ ($\mu V\ s^{-1}$) (**c**), (**d**) show dependence of the peak height on the square root of the potential scan rate for the oxidation peak

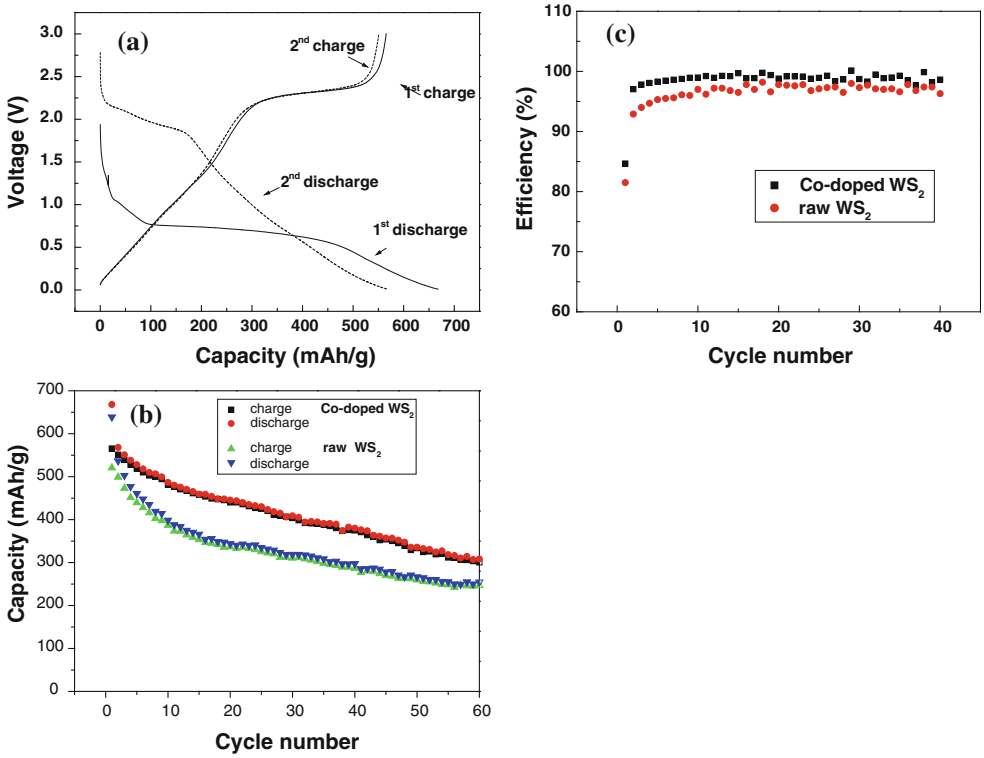

Fig. 6 Typical first and second charge/discharge curves of the Co-doped WS_2 electrode (**a**), typical cycling performance of the precursor WS_2 and the as-prepared Co-doped WS_2 electrode (**b**) and coulombic efficiency versus cycle number of the raw and Co-doped WS_2 (**c**). Current density: 50 mA g^{-1}

lamellae or monolayers by *n*-butyllithium to form Li_xWS_2, with the process introducing a large amount of defects, along with large changes in the coordination patterns of the lamellar disulfide, which enables doping with other ions. Then, the $CoCl_2$ aqueous solution is added into the above mixture, a dispersion of single-layer WS_2 is formed by the reaction of Li_xWS_2 with water. After Co^{2+} cations enter into the WS_2 matrix, the bonding properties of the matrix

and the bond angles of S–W–S are changed, especially on the sides of layers, which causes the lamellar structure to curl into bamboo-like nanorods.

The decreased capacity of this transition metal-doped WS_2 electrode may be because the intercalation of transition metal ions into the WS_2 matrix can decrease the distance between layers, which limits the amount of lithium ions electrochemically inserted into the Co-doped WS_2. Based on previous research [19–21], lithium ions intercalate into WS_2 nanoclusters and defect sites in WS_2 nanorods, but these sites are partly saturated with Co^{2+}, so the amount of intercalation of lithium ions will be decreased, and the capacity could thus also be decreased. It can be deduced that for WS_2 samples without transition metal-doping or mesoporous WS_2, this exfoliation–restacking method will both enhance the charge/discharge capacity and achieve better WS_2 cycling stability. Further work is needed in order to further improve the electrochemical performance of WS_2 samples via exfoliation and restacking, as well as other modifications.

Conclusions

Bamboo-like Co-doped WS_2 nanorods were synthesized by an exfoliation–intercalation–hydrothermal method. WS_2 powder was used as the precursor and was exfoliated by *n*-butyllithium. Co^{2+} cations were doped into the WS_2 matrix through a hydrothermal process in $CoCl_2$ aqueous solution. This method is expected to be applied to other layered materials to obtain the desired morphologies. The Co-doped WS_2 nanorods can reversibly store lithium with a capacity of 568 mAh g^{-1} over a voltage range of 0.01–3.0 V versus Li/Li^+. The Co-doped WS_2 electrode shows much better cycling stability compared with the raw WS_2 electrode.

Acknowledgments This work was supported partially by the State Key Laboratory Breeding Base of Green Chemistry-Synthesis Technology, Zhejiang University of Technology and the Priority Research Centers Program through the National Research Foundation of Korea (NRF) funded by the Ministry of Education, Science and Technology (2009-0094047).

References

1. M. Homyonfer, B. Alperson, Y. Rosenberg, L. Sapir, S.R. Cohen, G. Hodes et al., J. Am. Chem. Soc. **119**, 2693 (1997)
2. L. Rapport, Y. Bilik, Y. Feldman, M. Homyonfer, S.R. Cohen, R. Tenne, Nature **387**, 791 (1997)
3. M.M. Mdleni, T. Hyeon, K.S. Suslick, J. Am. Chem. Soc. **120**, 6189 (1998)
4. J. Chen, N. Kuriyama, H.T. Yuan, H.T. Takeshita, T. Sakai, J. Am. Chem. Soc. **123**, 11813 (2001)
5. H.B. Yang, S.K. Liu, J.X. Li, M.H. Li, G. Peng, G.T. Zou, Nanotechnology **17**, 1512 (2006)
6. J.J. Hu, J.S. Zabinski, J.H. Sanders, J.E. Bultman, A.A. Voevodin, J. Phys. Chem. B **110**, 8914 (2006)
7. L.L. Zhang, J.P. Tu, H.M. Wu, Y.Z. Yang, Mater. Sci. Eng. A **454–455**, 487 (2007)
8. X.W. Lou, C.C. Zeng, Chem. Mater. **14**, 4781 (2002)
9. D. Vollath, D.V. Szabo, Mater. Lett. **35**, 236 (1998)
10. N. Mirabal, V. Lavayen, E. Benavente, M.A. Santa Ana, G. Gonzalez, Microelectron J. **35**, 37 (2004)
11. B.A. Vanchura, P.G. He, V. Antochshuk, M. Jaroniec, A. Ferryman, D. Barbash, J. Am. Chem. Soc. **124**, 12090 (2002)
12. A.C. Bloise, J.P. Donoso, J. Phys. Chem. B. **106**, 11698 (2002)
13. J. Rouxel, Mater. Res. Bull. **13**, 1425 (1978)
14. Y.V. Zubavichus, Y.L. Slovokhotov, P.J. Schilling, Inorg. Chim. Acta **280**, 211 (1998)
15. Y.D. Li, X.L. Li, R.G. He, J. Zhu, Z.X. Deng, J. Am. Chem. Soc. **124**, 1411 (2002)
16. A.S. Golub, I.B. Shumilova, Y.V. Zubavichus, Yu.L. Slovokhotov, Yu.N. Novikov, A.M. Marie, M. Danot, Solid State Ionics **122**, 137 (1999)
17. G.H. Li, Z.D. Xu, W.X. Chen, Q.L. Nie, Chem. J. Chin. Univ. **24**, 2155 (2003)
18. S.Q. Wang, G.H. Li, Y.P. He, H.Y. Yin, Z.D. Xu, B.S. Zou, Mater. Lett. **60**, 815 (2006)
19. B.G. Sibernagel, Solid State Commun. **17**, 361 (1975)
20. C.Q. Feng, L.F. Huang, Z.P. Guo, H.K. Liu, Electrochem. Commun. **9**, 119 (2007)
21. G.X. Wang, S. Bewlay, J. Yao, H.K. Liu, S.X. Dou, Electrochem. Solid State Lett. **7**(10), A321–A323 (2004)
22. P. Poizot, S. Laruelle, S. Grugeon, L. Dupont, J.-M. Tarascon, Nature **407**, 496 (2000)
23. M. Virsek, A. Jesih, I. Milosevic, M. Damnjanovic, M. Remskar, Surf. Sci. **601**, 2868 (2007)
24. Q. Wang, J.H. Li, J. Phys. Chem. C. **111**, 1675 (2007)
25. M.D. Levi, D. Aurbach, J. Electroanal. Chem. **421**, 79 (1997)